J. Micromech. Microeng. **9** (1999) 64–70. Printed in the UK PII: S0960-1317(99)97876-2

Analysis and design of polysilicon thermal flexure actuator

Qing-An Huang† and Neville Ka Shek Lee‡

Department of Industrial Engineering and Engineering Management, The Hong Kong University of Science and Technology, Clear Water Bay, Hong Kong

Received 28 September 1998, in final form 21 December 1998

Abstract. An analytical model that can accurately predict the performance of a polysilicon thermal flexure actuator has been developed. This model is based on an electrothermal analysis of the actuator, incorporating conduction heat transfer. Heat radiation from the hot arm of the actuator to the cold arm is also estimated. Results indicate that heat radiation becomes significant only at high input power, and conduction heat losses to both the substrate and the anchor are mainly responsible for the operating temperature of the actuator under routine operations. Actuator deflection is computed based on elastic analysis of structures. To verify the validity of the model, polysilicon thermal flexure actuators have been fabricated and tested. Experimental results are in good agreement with theoretical predications except at high input power. An actuator with a 240 μm long, 2 μm thick, 3 μm wide hot arm and a 180 μm long, 12 μm wide cold arm deflected up to 12 μm for the actuator tip at an input voltage of 5 V while it could be expected to deflect up to 22 μm when a 210 μm long cold arm is used.

1. Introduction

In micromechanical structures, actuators based on electrostatic forces operate at low power and high frequency, and are highly desirable. However, they have typically small deflections and require either close dimensional tolerances or high voltage to achieve large deflections. On the other hand, actuators based on the thermal expansion effect can provide a large force and a deflection perpendicular [1] or parallel [2] to the substrate. They have been shown to be a valuable complement to electrostatic actuators [3, 4]. In particular, polysilicon thermal actuators can operate in an integrated circuit (IC) current/voltage regime and may be fabricated by a surface-micromachining technology that is compatible with IC technology [5, 6]. The operating principle of a thermally driven actuator with lateral motion (parallel to the substrate) is the asymmetrical thermal expansion of a microstructure with variable cross sections. The resistance of the narrower section of the microstructure is higher than that of the wider section. When current passes through the actuator, more power dissipates in the narrower section, causing it to expand more than the wider section. This differential thermal expansion may be compared to that of a bimorph structure, causing the actuator to move laterally. At the same time, this principle also renders the deflection of the actuator to be related to various process parameters, the physical geometry, and the driving current. The numerical simulation has been performed to optimize the actuator structure [6], while a parametric model of the actuator is essential and useful for practical applications. It is therefore the purpose of this paper to develop an analytical model so as to provide an insight into the operation of the actuator, and to allow for predicting the performance of actuators with new designs before fabrication. In section 2, the theoretical model is developed. The electrothermal performance of the actuator is first analysed, and the deflection characteristics of the actuator are then presented. In the following section on fabrication and test, polysilicon thermal actuators fabricated by a surface micromachining process are tested. The experimental results are compared to those of the analytical model. The latter is shown to have correctly predicted the deflections of the actuators. Finally, various design considerations such as physical geometry of the actuator are discussed in section 4, and a conclusion is summed up in section 5.

2. Theoretical model

A diagram of a polysilicon thermal actuator is shown in figure 1(a). It generates deflection through asymmetric heating of the hot and cold arms. Current is passed through the anchors, and the higher current density in the narrower hot arm causes it to heat and expand more than the wider cold arm. The arms are jointed at the free end which forces the actuator tip to move laterally in an arcing motion towards the cold arm side.

2.1. Electrothermal analysis

The electrothermal response of polysilicon microbeams is generally simplified for analysis in one dimension [7, 8]

† On leave from Microelectronics Center, Southeast University, Nanjing 210096, People's Republic of China.
‡ Corresponding author. Tel: (852) 2358 7104. Fax: (852) 2358 0062. E-mail address: nlee@ust.hk.

0960-1317/99/010064+07$19.50

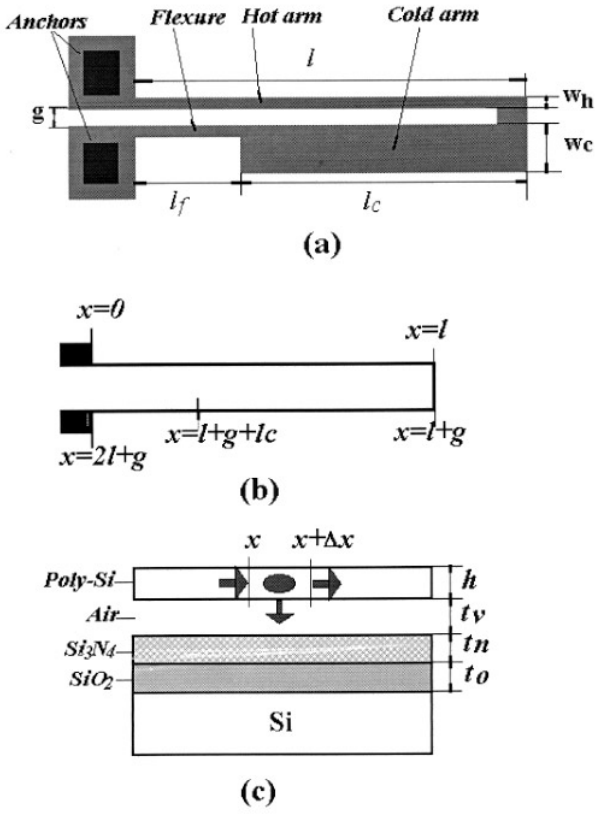

Figure 1. (a) Schematic top view of polysilicon thermal flexure actuator. (b) Simplified one dimensional coordinate system. (c) Cross-section diagram of the actuator for thermal analysis.

since the size in the length direction is much larger than that of its cross-section. The arms of the actuator shown in figure 1(a) may be decomposed into three lineshape microbeams connected in series. The coordinate system for thermal analysis is given in figure 1(b). A part of the cross-section of the actuator is shown in figure 1(c). The silicon nitride and oxide layers shown in this figure are used as electrical and thermal insulation.

The resistivity of polysilicon, ρ, is usually related to temperature. The resistivity is assumed here to have a linear temperature coefficient, ξ, such that $\rho\,(T_s) = \rho_0$, that is,

$$\rho\,(T) = \rho_0\,[1 + \xi\ \ (T - T_s)] \tag{1}$$

where T is the operating temperature, and T_s is the substrate temperature. As shown in figure 1(c), the heat flow equation is derived by examining a differential element of the microbeam of width w, thickness h and length Δx. Under steady-state conditions, resistive heating power generated in the element is equal to heat conduction out of the element.

$$-k_p wh\left[\frac{\mathrm{d}T}{\mathrm{d}x}\right]_x + J^2\rho\, wh\Delta x = -k_p wh\left[\frac{\mathrm{d}T}{\mathrm{d}x}\right]_{x+\Delta x} + S\Delta x w\frac{T - T_s}{R_T} \tag{2}$$

where k_p is the thermal conductivity of polysilicon, J is the current density, S is the shape factor which accounts for the impact of the shape of the element on heat conduction to the substrate and R_T would be the thermal resistance between the polysilicon microbeam and the substrate if the microbeam were wide enough. R_T is given by

$$R_T = \frac{t_v}{k_v} + \frac{t_n}{k_n} + \frac{t_o}{k_o} \tag{3}$$

where t_v, t_n and t_o are the elevation of the element above the Si_3N_4 surface, the thickness of Si_3N_4 and the thickness of SiO_2, respectively and, k_v, k_n and k_o are the thermal conductivity of air, Si_3N_4 and SiO_2, respectively. The shape factor for heat conduction is given by [8]

$$S = \frac{h}{w}\left(\frac{2t_v}{h} + 1\right) + 1. \tag{4}$$

Taking the limit as $\Delta x \to 0$ for equation (2) produces the following second-order differential equation.

$$k_p\frac{\mathrm{d}^2T}{\mathrm{d}x^2} + J^2\rho = \frac{S}{h}\frac{(T - T_s)}{R_T}. \tag{5}$$

Physically, the first term on the left side of equation (5) represents the net rate of heat conduction into the element per unit volume. The second term on the left side is the rate of heat energy generation inside the element per unit volume, and the right side represents the rate of heat energy loss in the element per unit volume. Changing variables for equation (5) with equation (1) yields

$$\frac{\mathrm{d}^2\theta(x)}{\mathrm{d}x^2} - m^2\theta(x) = 0 \tag{6}$$

with

$$\theta\ (x) = T(x) - T_\theta$$

$$T_\theta = T_s + \frac{J^2\rho_0}{k_p m^2}$$

$$m^2 = \frac{S}{k_p h R_T} - \frac{J^2\rho_{\,0}\xi}{k_p}.$$

Solving equation (6) and applying the solution to the hot arm, cold arm and flexure, one obtains the temperature distribution as follows, respectively.

$$T_h(x) = T_H + c_1\,\mathrm{e}^{m_h x} + c_2\,\mathrm{e}^{-m_h x} \tag{7}$$

$$T_c(x) = T_C + c_3\,\mathrm{e}^{m_c x} + c_4\,\mathrm{e}^{-m_c x} \tag{8}$$

$$T_f(x) = T_F + c_5\,\mathrm{e}^{m_f x} + c_6\,\mathrm{e}^{-m_f x} \tag{9}$$

where T_H and m_h are the same as T_θ and m, respectively, except that w is replaced by w_h; T_C and m_c are the same as T_θ and m, respectively, except that w is replaced by w_c; w_h and w_c are the widths of the hot and cold arms, respectively, c_j ($j = 1$ to 6) are the constants to be solved, $T_F = T_H$ and $m_f = m_h$ since the width of the flexure is the same as that of the hot arm.

The anchor pads are assumed to have the same temperature as the substrate. Utilizing the continuity of both the temperature and the rate of heat conduction across the joint points of the hot arm, cold arm and flexure, one obtains the following equation to solve the constants c_j ($j = 1$ to 6)

Table 1. Parameters used in this analysis.

Parameter	Value
Young' modulus of polysilicon, E	150×10^9 Pa
Thermal expansion of polysilicon, α	2.7×10^{-6} °C^{-1}
Effective absorptivity of polysilicon, ε	0.6
Thermal conductivity of polysilicon, k_p	30 W m^{-1} °C^{-1}
Thermal conductivity of air, k_v	0.026 W m^{-1} °C^{-1}
Thermal conductivity of Si_3N_4, k_n	2.25 W m^{-1} °C^{-1}
Thermal conductivity of SiO_2, k_o	1.4 W m^{-1} °C^{-1}
Substrate temperature, T_s	20 °C

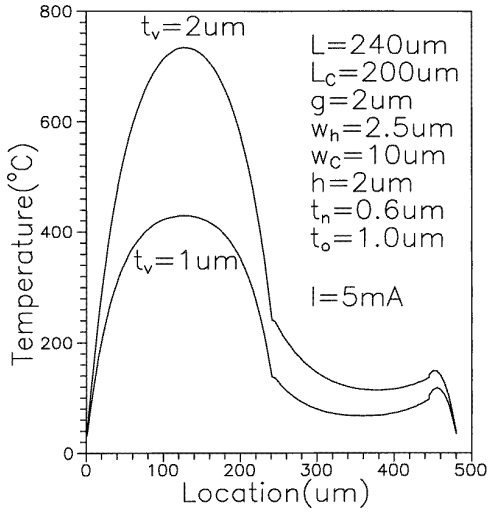

Figure 2. Temperature distribution along the polysilicon arm for two different elevations of the polysilicon arm above the substrate with $\rho_0 = 1.0 \times 10^{-3}\ \Omega$ cm and $\xi = 1.25 \times 10^{-3}$ °C^{-1}.

$$\overline{T}_h = T_H + \frac{c_1}{m_h L}\left(e^{m_h L} - 1\right) - \frac{c_2}{m_h L}\left(e^{-m_h L} - 1\right) \tag{12}$$

$$\overline{T}_c = T_C + \frac{c_3}{m_c(L_c + g)}\left(e^{m_c(L+g+L_c)} - e^{m_c L}\right) - \frac{c_4}{m_c(L_c + g)}\left(e^{-m_c(L+g+L_c)} - e^{-m_c L}\right) \tag{13}$$

$$\overline{T}_f = T_H + \frac{c_5}{m_h L_f}\left(e^{m_h(2L+g)} - e^{m_h(L+g+L_c)}\right) - \frac{c_6}{m_h L_f}\left(e^{-m_h(2L+g)} - e^{-m_h(L+g+L_c)}\right). \tag{14}$$

The linear thermal expansion for the hot arm, cold arm and flexure, which is to be used later to estimate the deflection of the actuator, may be calculated as, respectively,

$$\Delta L_h = \alpha \int_0^L (T_h(x) - T_s)\,\mathrm{d}x = \alpha\, L(\overline{T}_h - T_s) \tag{15}$$

$$\Delta L_c = \alpha \int_L^{L+g+L_c} (T_c(x) - T_s)\,\mathrm{d}x = \alpha\, L_c(\overline{T}_c - T_s) \tag{16}$$

$$\Delta L_f = \alpha \int_{L+g+L_c}^{2L+g} (T_f(x) - T_s)\,\mathrm{d}x = \alpha\, L_f(\overline{T}_f - T_s) \tag{17}$$

where α is the thermal expansion coefficient of polysilicon. The thermal expansion due to the section of gap has been ignored in equation (16) because of its short length.

$$\begin{bmatrix} 1 & 1 & 0 & 0 & 0 & 0 \\ e^{m_h L} & e^{-m_h L} & -e^{m_c L} & -e^{-m_c L} & 0 & 0 \\ e^{m_h L} & -e^{-m_h L} & -\lambda\, e^{m_c L} & \lambda\, e^{-m_c L} & 0 & 0 \\ 0 & 0 & e^{m_c(L+g+L_c)} & e^{-m_c(L+g+L_c)} & -e^{m_h(L+g+L_c)} & -e^{-m_h(L+g+L_c)} \\ 0 & 0 & \lambda\, e^{m_c(L+g+L_c)} & -\lambda\, e^{-m_c(L+g+L_c)} & -e^{m_h(L+g+L_c)} & e^{-m_h(L+g+L_c)} \\ 0 & 0 & 0 & 0 & e^{m_h(2L+g)} & e^{-m_h(2L+g)} \end{bmatrix} \begin{bmatrix} c_1 \\ c_2 \\ c_3 \\ c_4 \\ c_5 \\ c_6 \end{bmatrix} = \begin{bmatrix} T_s - T_H \\ T_C - T_H \\ 0 \\ T_H - T_C \\ 0 \\ T_s - T_H \end{bmatrix} \tag{10}$$

where L and L_c are the lengths of the hot and cold arms, respectively, g is the gap between the hot and cold arms, $\lambda = w_c m_c / w_h m_h$. The above equation (10) is written as a matrix format so that one may use the same subroutine as the deflection analysis to solve the linear algebraic equation. Once c_j ($j = 1$ to 6) are obtained, the resistance of polysilicon, which depends on temperature changes, may be estimated as follows

$$R = \int_0^{2L+g} \mathrm{d}R(T) = \frac{L\rho_0}{w_h h}\left[1 + \xi\,(\overline{T}_h - T_s)\right] + \frac{(L_c + g)\rho_0}{w_c h}\left[1 + \xi\,(\overline{T}_c - T_s)\right] + \frac{L_f \rho_0}{w_h h}\left[1 + \xi\,(\overline{T}_f - T_s)\right] \tag{11}$$

where $\overline{T}_h$, $\overline{T}_c$ and $\overline{T}_f$ stand for the average temperature of the hot arm, cold arm and flexure, respectively, and they can be expressed as

For the given process parameters such as ρ_0 and ξ, physical geometry and driving current, the temperature distribution can be obtained by equations (7)–(10). Figure 2 shows an example of the temperature distribution for the parameters specified in the figure. Other physical constants are listed in table 1. It is clear from this figure that the temperature in most of the hot arm is much higher than that in the cold arm. It is also obvious that heat loss due to conduction to the substrate affects strongly the temperature in the arms of the actuator. As shown in equation (3), the elevation (t_v) of the polysilicon arm above the substrate governs heat loss to the substrate since the thermal conductivity of air is very small. It has been shown that a trench etched under the hot arm of the actuator increases the thermal isolation from the substrate, thereby decreasing the heat loss from the hot arm and increasing the deflection [3].

As presented in the above, the thermal analysis performed for the actuator is based on heat conduction. At

higher power, however, heat loss due to thermal radiation may become significant. Especially, the heat radiative transfer from the hot arm to the cold one may give rise to increase of the cold arm temperature. It is therefore interesting to compare the heat energy generation due to resistive heating inside the cold arm with the heat radiative energy from the hot arm to the cold one. Both the resistive heating energy and the accepted radiative energy inside the cold arm tend always to increase its temperature. To simplify the estimation of the radiative energy, the average of the temperature in the hot and cold arms is used here.

The radiative energy received by the cold arm from the hot one may be approximately written as [9]

$$E_{hc} = hL_c F_{hc} \varepsilon \sigma \left(\overline{T}_h^4 - \overline{T}_c^4\right) \tag{18}$$

where ε is the effective absorptivity (or emissivity) of polysilicon, σ is the Stefan–Boltzman constant and F_{hc} is the radiation shape factor, which is given by [9]

$$\begin{aligned} F_{hc} = \frac{2}{\pi XY}\Bigg[& \ln\sqrt{\frac{\left(1+X^2\right)\left(1+Y^2\right)}{1+X^2+Y^2}} \\ & + X\sqrt{1+Y^2}\tan^{-1}\left(\frac{X}{\sqrt{1+Y^2}}\right) \\ & + Y\sqrt{1+X^2}\tan^{-1}\left(\frac{Y}{\sqrt{1+X^2}}\right) \\ & - X\tan^{-1}(X) - Y\tan^{-1}(Y)\Bigg] \end{aligned} \tag{19}$$

where $X = h/g$, $Y = L_c/g$.

The heat energy due to the resistive heating inside the cold arm is given by

$$E_G = J_c^2 \rho_0 \left[1 + \xi\ \left(\overline{T}_c - T_s\right)\right] hL_c w_c. \tag{20}$$

The ratio of E_G to E_{hc} as a function of the input power is shown in figure 3 for different gaps and cold arm widths. It can be seen that the smaller the gap, the stronger the radiation from the hot arm to the cold one for the same cold arm width. Also, the wider the cold arm, the lower the resistive heating energy due to the current density. Even at the power of 30 mW, the heat energy due to the resistive heating inside the cold arm is about 28 times higher than that due to the radiation from the hot arm. However, the radiative energy from the hot arm to the cold one may become significant at higher input power. Also, the thermal radiation to air from the local region of the hot arm, where the temperature is very high, becomes larger at higher input power. The thermal expansion for the hot arm is smaller than could be expected due to the thermal radiation from the hot arm to the air. The influence of the thermal radiation on the deflection of the actuator is to be ignored later in this paper because the actuators are usually not designed for routine operation at powers high enough to generate substantial thermal radiation. Moreover, irreversible changes in the polysilicon structure and actuator resistance may occur when high drive voltages are used.

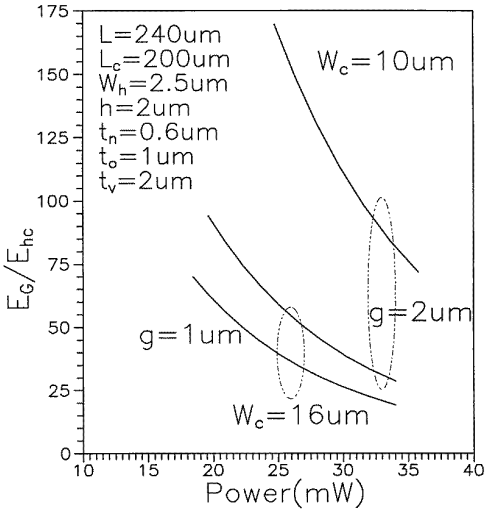

Figure 3. The ratio of the resistive heating energy inside the cold arm to the received radiative energy from the hot arm as a function of input power for different gaps and cold arm widths.

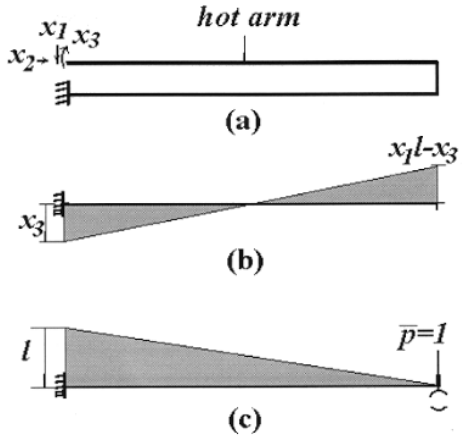

Figure 4. (a) The rigid frame simplified for the thermal actuator with three redundants. (b) The bending moment of the hot arm due to the thermal expansion of the structure. (c) The bending moment of the hot arm due to the virtual force.

2.2. Deflection analysis

The structure of the thermal actuator shown in figure 1 is similar to a plane rigid frame with two bases fixed for structural engineering [10]. Deflection analysis of the plane rigid frame has been well established in structural engineering. The thermal actuator in figure 1 is a statically indeterminate structure with the degree of indeterminacy being 3. The force method for the structural engineering is first used here to analyse the bending moment of the actuator structure due to the three redundants, X_1, X_2 and X_3, as shown in figure 4(a) where X_1 stands for a horizontal force, X_2 a vertical force and X_3 a couple force. The virtual-work method for structural engineering is then utilized to estimate the deflection of the actuator tip.

Following the force method [10], the three redundants, X_1, X_2 and X_3 can be obtained by solving a set of

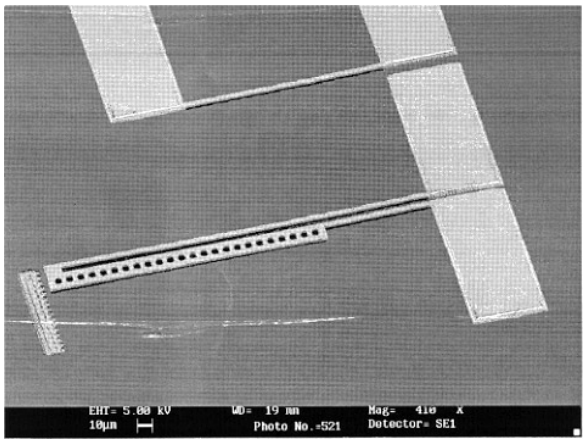

Figure 5. SEM picture of a polysilicon thermal actuator and a single beam used to measure the polysilicon resistivity and its temperature coefficient. Dimples inside the cold arm of the actuator prevent stiction to the substrate.

simultaneous equations:

$$\begin{bmatrix} f_{11} & f_{12} & f_{13} \\ f_{21} & f_{22} & f_{23} \\ f_{31} & f_{32} & f_{33} \end{bmatrix} \begin{bmatrix} X_1 \\ X_2 \\ X_3 \end{bmatrix} = \begin{bmatrix} 0 \\ \Delta L_h - \Delta L_c - \Delta L_f \\ 0 \end{bmatrix} \tag{21}$$

where terms f_{ij} represent flexibility coefficients, which can be easily obtained by the diagram product of the bending moments due to respective three unit redundants, X_1, X_2 and X_3. They are given by, respectively,

$$f_{11} = \frac{1}{3EI_h}\left(L^3 + L_f^3\right) + \frac{1}{3EI_c}\left(3L^2 g + L^3 - L_f^3\right) \tag{22a}$$

$$f_{12} = f_{21} = -\frac{1}{2EI_h}\left(L_f^2 g\right) - \frac{1}{2EI_c}\left(g^2 L + L^2 g - L_f^2 g\right) \tag{22b}$$

$$f_{13} = f_{31} = -\frac{1}{2EI_h}\left(L^2 + L_f^2\right) - \frac{1}{2EI_c}\left(L^2 + 2Lg - L_f^2\right) \tag{22c}$$

$$f_{22} = \frac{1}{3EI_c}\left(g^3 + 3L_c g^2\right) + \frac{1}{EI_h}\left(L_f g^2\right) \tag{22d}$$

$$f_{23} = f_{32} = \frac{1}{2EI_c}\left(g^2 + 2gL_c\right) + \frac{1}{EI_h}\left(gL_f\right) \tag{22e}$$

$$f_{33} = \frac{1}{EI_h}\left(L + L_f\right) + \frac{1}{EI_c}\left(L_c + g\right) \tag{22f}$$

where E is the Young's modulus of polysilicon, I_h ($= hw_h^3/12$) is the moment of inertia for the hot arm, I_c ($= hw_c^3/12$) is the moment of inertia for the cold arm, EI_h and EI_c represent the flexural rigidity of the hot and cold arms, respectively. The three redundants, X_1, X_2 and X_3 may be solved by equation (21). Once they are obtained, the bending moment of the hot arm due to the thermal expansion can be represented as in figure 4(b). In order to obtain the deflection of the actuator tip, a virtual unit force $\boldsymbol{P}$ is applied to the free end of the actuator. The bending moment of the hot arm due to the virtual force is shown in figure 4(c). According to the method of virtual work [10], the deflection in the free end of the actuator can be written as

$$u = \int \frac{\overline{M}M}{EI_h}\,\mathrm{d}s = \frac{L^2}{6EI_h}\left(X_1 L - 3X_3\right) \tag{23}$$

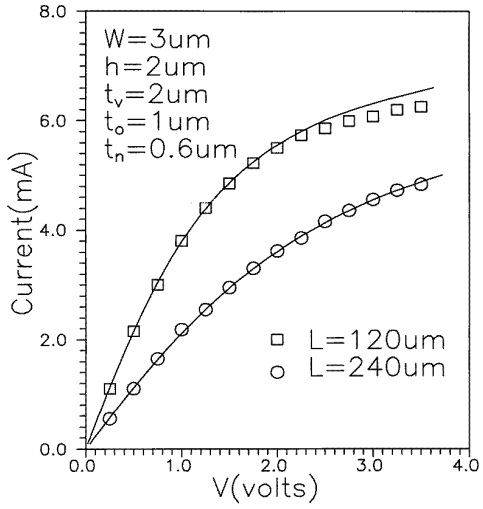

Figure 6. I–V curves of a single polysilicon beam. Solid lines represent the theoretical results.

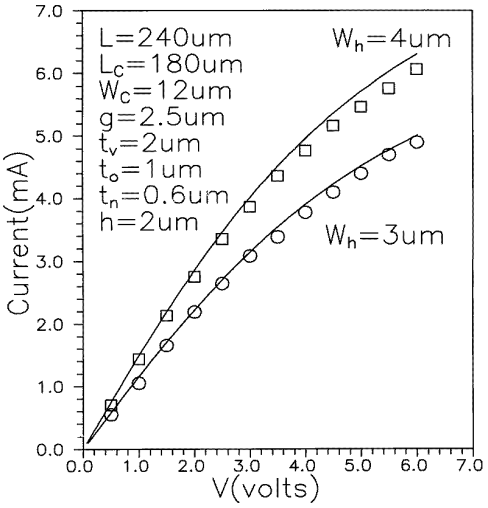

Figure 7. I–V curves of polysilicon thermal actuators for different widths of the hot arm. Solid lines represent the theoretical results.

where M is the bending moment (figure 4(b)) due to the thermal expansion, $\overline{M}$ represents the bending moment (figure 4(c)) due to the unit virtual force.

3. Fabrication and test

The thermal actuators in this study were fabricated by a polysilicon surface micromachining technology. A set of actuators with different physical dimensions were fabricated on the same chip. The SiO_2, Si_3N_4, sacrificial PSG (phosphorus-doped glass) and polysilicon layers were all deposited by LPCVD (low pressure chemical vapour deposition). The thickness of the SiO_2, Si_3N_4, PSG and polysilicon layers is 1, 0.6, 2 and 2 μm, respectively. Heavily phosphorus-doped (approximately 10^{20} atoms cm^{-3}) polysilicon was grown by an LPCVD *in situ* phosphorus-doping process. After construction, the actuators were released by removing the sacrificial PSG layer in a bath

of buffered hydrofluoric acid (BHF). The wafer was rinsed repeatedly with DI water for 30 minutes after the BHF was completed and it was then immersed in isopropanol for 10 minutes. Finally, it was dried in a standard spin dryer. Figure 5 is an SEM micrograph of the actuator. A built-in scale next to the actuator tip is used to measure the actuator deflection. A single beam adjacent to the actuator is used to measure the resistivity of polysilicon and its temperature coefficient to avoid inaccuracy of the resistance of the actuator due to dimples inside the cold arm. Basic electrothermal characteristics have been studied by comparing theoretical and experimental I–V curves in an air environment. Figure 6 shows measurement results of I–V curves for the single beam of polysilicon. In figure 6, L, W and h stand for the length, width and thickness of the single beam of polysilicon, respectively. Solid lines in figure 6 are theoretical results according to our analytical model. It is found by the best curve-fitting method that the resistivity of polysilicon (ρ_0) is 1.1×10^{-3} Ω cm, and its temperature coefficient (ξ) is 1.3×10^{-3} $^\circ\mathrm{C}^{-1}$. Figure 7 shows the experimental and theoretical I–V curves of the actuators. The polysilicon resistivity and its temperature coefficient obtained for the single beam are used in equation (11) to generate those theoretical curves. Good agreement is observed between them except that the input current is higher. At higher current, deviations of theoretical results from the experimental data may result from heat loss due to the thermal radiation in the hot arm. On the other hand, the thermal conductivity for polysilicon and air, which is temperature dependent, is theoretically treated here as constant. This may also be a cause. Deflection as a function of the external voltage was measured shown for different widths of the hot arm. Theoretical results show that the deflection of the actuator with $w_h = 3$ μm is a little larger than that for $w_h = 4$ μm. However, the experimental results may not distinguish $w_h = 3$ μm from $w_h = 4$ μm. Figure 8 shows the deflection as a function of the input current. It can be seen from this figure that the deflection of the actuator for $w_h = 3$ μm is larger than that for $w_h = 4$ μm at the same input current. The reason is that the deflection of the actuator depends on the net thermal expansion of the hot arm, cold arm and flexure as well as the flexural rigidity of the arms. The current density of the hot arm for $w_h = 3$ μm is higher than that for $w_h = 4$ μm at the same input current. Deflection as a function of the external voltage is shown in figure 9 for different lengths of the cold arm. It is clear that the longer the cold arm, the bigger the deflection of the actuator at the same voltage. It will be later discussed that the situation is not always like this. The deflection as a function of the external voltage for different gaps was measured to show that at the same voltage the smaller gap enabled the actuator to deflect more if the radiation from the hot arm to the cold one is not high (e.g. at low input power). Comparison of theoretical results with experimental data shows a good agreement between them except at high input current.

4. Discussion

The performance of a polysilicon thermal actuator is related to process parameters and geometry as well as input power.

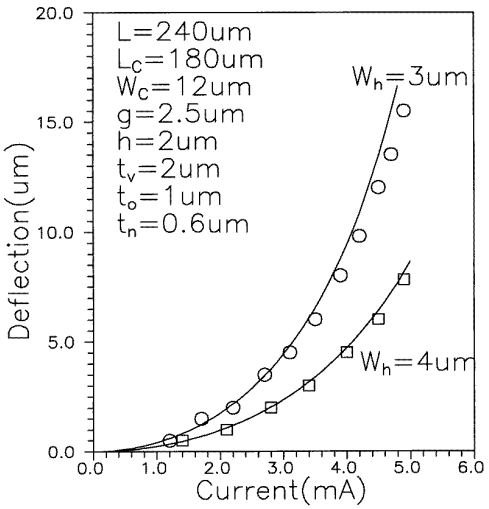

Figure 8. Deflection of the actuator tip as a function of the input current for different widths of the hot arm. Solid lines represent the theoretical results.

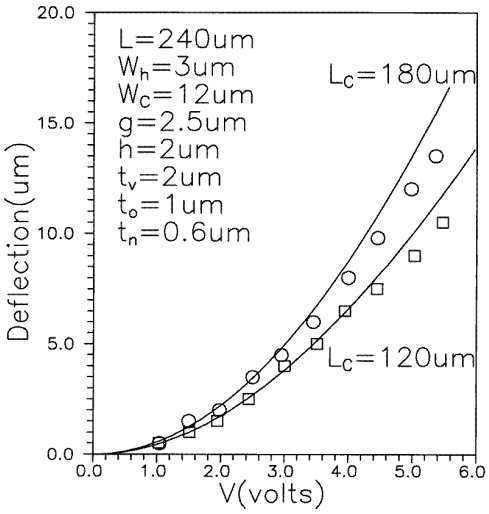

Figure 9. Deflection of the actuator tip as a function of the voltage for different lengths of the cold arm. Solid lines represent the theoretical results.

Their relationships have been developed in the above. Such relationships operate well except at high input power. In general, it is desired to design a polysilicon thermal actuator with large deflection. Hence, deflection as a function of geometry is studied here based on the above analytical model. In figure 10, deflection as a function of the length ratio of the cold arm to the hot one is plotted for different widths of the cold arm at an input current of 5 mA. It can be seen that the length ratio has a significant influence on the actuator deflection. The net thermal expansion responsible for the deflection of the actuator increases with length ratio, while the contribution of the flexural rigidity of the cold arm to the bending of both the cold arm and the flexure also increases with length ratio. As a result, there is a maximum in deflection. It is obvious that no deflection occurs when $L_c = 0$, due to no net expansion. At the same ratio of cold arm to hot arm, the wider the cold arm, the larger the deflection, as the average temperature for a wider cold arm is

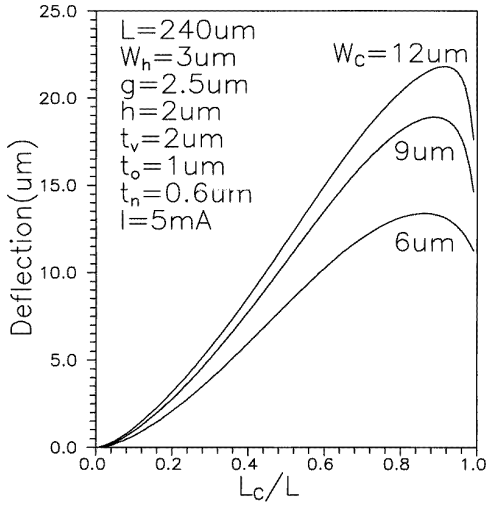

Figure 10. Deflection as a function of the length ratio of the cold arm to the hot one for different widths of the cold.

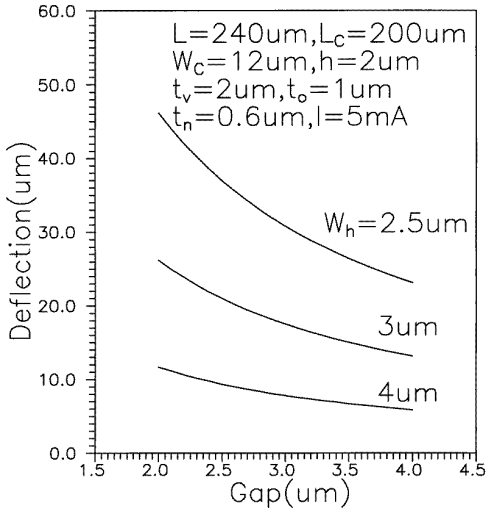

Figure 11. Deflection as a function of the gap for different widths of the hot arm.

lower than that for a narrower one at the same input current. In figure 11, deflection as a function of the gap between the hot and cold arms is shown for different widths of the hot arm. As shown in this figure, deflection of the actuator decreases with increasing the gap. It is therefore desired to narrow the gap in a process to achieve larger deflections. As shown in figure 3, however, heat radiation from the hot arm to the cold one becomes significant for a narrower gap, meaning that the temperature of the cold arm will be elevated and thus the deflection reduced. For the same gap, deflection of the actuator decreases with increasing the width of the hot arm, due to both the current density and the flexural rigidity of the hot arm. The deflection as a function of the hot arm length is estimated to show that deflection of the actuator increases obviously with the hot arm length. It is therefore desired to design longer hot arms so as to achieve a larger deflection. However, the tradeoff lies in that electrical resistance also increases with the length of the hot arm; so does the chance of the actuator failure due to stiction of a longer arm to the substrate during fabrication. Also, a longer hot arm is likely to deliver less force because of bowing [5]. The deflection of the actuator decreases with increasing the thickness of the arm for the same input current because of a lower input current density. Various process parameters such as resistivity also have effects on actuator deflection. For example, at the same voltage, one may obtain a larger deflection for arms with higher resistivity.

5. Conclusion

An electrothermal model for polysilicon thermal flexure actuators has been developed based on heat conduction. Heat radiation from the hot arm of the actuator to the cold one has also been estimated. It is shown that heat radiation becomes important for the operation of the actuator only at high input power. Deflection of the actuator has been presented, based on an elastic analysis of structures. As a measure to verify our theoretical model, actual deflections in polysilicon thermal actuators have been measured and compared with the results of the theoretical model. Good agreement has been achieved. The theoretical model presented would therefore find applications in the design and optimization of polysilicon thermal flexure actuators.

Acknowledgment

This research was supported in the past by the RIG grant of Hong Kong University of Science and Technology.

References

[1] Riethmuller W and Benecke W 1988 Thermally excited silicon microactuators *IEEE Trans. Electron Devices* **35** 758–63

[2] Guckel H, Klein J, Christen T, Skrobis K, Landon M and Lovell E G 1992 Thermo-magnetic metal flexure actuators *Tech. Digest IEEE Solid State Sensor and Actuator Workshop* pp 73–5

[3] Field L A, Burriesci D L, Robrish P R and Ruby R C 1996 Micromachined 1×2 optical fiber switch *Sensors Actuators* A **53** 311–5

[4] Noworolski J M, Klaassen E H, Logan J R, Peterson K E and Maluf N I 1996 Process for in-plane and out-plane single crystal silicon thermal microactuators *Sensors Actuators* A **55** 65–9

[5] Comtois J H and Bright V M 1997 Applications for surface-micromachined polysilicon thermal actuators and arrays *Sensors Actuators* A **58** 19–25

[6] Pan C S and Hsu W 1997 An electro-thermally and laterally driven polysilicon microactuator *J. Micromech. Microeng.* **7** 7–13

[7] Fedder G K and Howe R T 1991 Thermal assembly of polysilicon microstructures *Proc. IEEE Micro Electro Mechanical System Workshop* pp 63–8

[8] Lin L and Chiao M 1996 Electrothermal response of lineshape microstructures *Sensors Actuators* A **55** 35–41

[9] Carslaw H S and Jaeger J C 1959 *Conduction of Heat in Solids* 2nd edn (London: Oxford University Press)

[10] Kennedy J B and Madugula M K S 1990 *Elastic Analysis of Structures* (New York: Harper and Row) ch. 7, 9